2021 IEEE/RSJ International Conference on Intelligent Robots and Systems (IROS)
September 27 - October 1, 2021. Prague, Czech Republic

An Analysis on the Modeling Accuracy of Industrial Manipulators with Inherent Joint Elasticity

Rajesh Subburaman[1], Mariapaola D'Imperio[1], Jinoh Lee[2], and Ferdinando Cannella[1]

Abstract— **High precision industrial applications call for equally precise functioning of industrial manipulators, which in turn requires accurate modeling of the manipulators. This paper carries out a detailed study on the modeling of industrial manipulators with elastic joints to improve their accuracy. In particular, the effect of adopting a simple harmonic drive (HD) model and ignoring a dynamic effect called *low inertia coupling* between the actuators and links on the model accuracy has been analyzed from a parameter estimation perspective. Since the aforementioned model characteristics have been generally ignored for high gear reduction ratios, this study is carried out with five different reduction ratios ranging from low to high, where three different models of a three-joints elastic manipulator are considered. The accuracy of the models is compared using the torque performance metrics of a predefined joint motion of the robot. Furthermore, the impact of the models with different accuracy is assessed by carrying out a state-of-the-art dynamic parameter estimation, and the resulting errors are compared to ascertain the merits of adopting a detailed elastic dynamic model of a manipulator.**

Keywords – **Flexible joints, Dynamic model, Modelling errors, Manipulators, Parameter estimation.**

I. Introduction

In modern days, industrial manipulators play a vital role to achieve quality products at low cost and time. The growing demand for quality particularly increases the need for accuracy in manipulator applications. In robotic measurement applications, the accuracy requirements for manipulators are even greater, in the order of [μm]. These requirements can only be met with accurate dynamic models that can facilitate precise pose estimation and control of manipulators. Lately, to reduce the overall cost of operation and for safety concerns, lightweight and elastic manipulators are mostly sought after. The inclusion of elasticity makes it even more challenging to model the non-linear dynamics of a manipulator with high accuracy and to control it effectively.

Several types of models have been used to represent the dynamics of industrial manipulators and estimate their corresponding parameters to simulate their dynamic motion. The most common one is a rigid body model, which assumes the joints and links to be rigid. This model has been used extensively in many parameters estimation works [1]–[6] to estimate the various inertial parameters—mass, center of mass, and inertia of each link. Interestingly, in [7], by ignoring some dynamic terms and estimating link-side torques, an elastic joint model is adapted to make use of the rigid joint model structure to estimate inertial parameters. On the other hand, citing the insufficiency of the rigid body models to accurately capture highly non-linear dynamics of manipulator systems, several different types of works have been proposed to enhance the model accuracy: in [8], the parameters are estimated offline using the rigid body models and further tuned online using a neural network to capture the dynamics which is not represented by the models. Although such online tuning approach has been fairly successful, it requires a large amount of data that encompasses different movements of the robot, which is difficult to achieve in practice; and as an alternative, online adaptive controllers have been proposed to compensate for the model inaccuracy, as reported in [9].

Since most of the robot's joints have inherent elasticity stemming from the transmission elements such as harmonic drives and belt-pulley, an elastic joint model has been considered in some parameter estimation works. In [10], a simplified elastic joint model for a single joint has been considered to estimate the inertia, joint elasticity, and actuator parameters, separately for each joint. The estimated parameters are validated with a 7 degrees-of-freedom (DoF) DLR light-weight robot by performing several point-point constant velocity movements, and the results are shown to be good. However, no quantitative data on the end-effector's accuracy has been reported. Unlike [10] where only drive flexibility has been considered, authors in [11]–[13] additionally consider flexibility in the joint due to bearings to further increase the accuracy of the elastic models. The dynamic characteristics of the model with estimated parameters are verified using frequency response functions (FRF) between motor torques (input) and its corresponding speeds (output). A close correspondence between the experimental and predicted FRF matrices along the diagonal terms has been reported in [11], [12], but the off-diagonal terms vary considerably, which suggests that the dynamic effects of distal links on a particular joint are not captured accurately by the model. Nevertheless, in [12], which also considers joint offset, misalignment, gear backlash, and kinematic parameters, the maximum absolute error of the end-effector with the estimated parameters is reported to be 0.32 mm over 150 different poses.

The use of elastic models in the aforementioned works is more likely to represent the robot dynamics closely when compared to those with rigid dynamic models. However, the

[1]Authors are with the Industrial Robotics Unit, Istituto Italiano di Tecnologia (IIT), Via Morego 30, 16163, Genova, Italy (email:{rajesh.subburaman, mariapaola.dimperio, ferdinando.cannella}@iit.it)

[2]Jinoh Lee is with the Institute of Robotics and Mechatronics, German Aerospace Center (DLR), 82234 Weßling, Germany (email:jinoh.lee@dlr.de)

reported accuracy of the former models is still insufficient for measurement applications which demand high accuracy than precision, e.g., inspection of manufactured parts. While moderately precise manipulators can be achieved with fairly accurate models and controllers, to obtain high accuracy, it is necessary to have highly accurate robot models. This calls for pushing the accuracy of elastic models even further. Interestingly and importantly, a closer look at the aforementioned elastic models reveals the following facts:

1) a simplified version of the complete elastic model ignored the low inertia coupling terms between the link and actuator dynamics; and
2) no separate model has been considered for the transmission system elements.

Both the facts are based on the assumption that the additional torque contributed by them is relatively small due to high joint reduction ratios, and doing so simplifies the model.

Accordingly, this study aims at understanding the effects of ignoring low inertia coupling terms and transmission system models on the robot's model accuracy, and thereby, propose an elastic manipulator model which can potentially improve the model's accuracy. In particular, the work makes the following contributions: 1) a detailed elastic model error analysis of ignoring low inertia coupling terms and adopting a simple HD model; 2) the aforementioned error analysis repeated across a range of transmission ratios to understand its effect and to quantify the resulting error; and 3) impact of less accurate elastic models of a manipulator on the estimation of its dynamic parameters/coefficients.

II. Problem Description

The dynamic equations of motion for an elastic joint robot in its general form can be written as given in [14] as follows:

$$\begin{pmatrix} \mathbf{M}(\mathbf{q}) & \mathbf{S}(\mathbf{q}) \\ \mathbf{S}^T(\mathbf{q}) & \mathbf{B} \end{pmatrix} \begin{pmatrix} \ddot{\mathbf{q}} \\ \ddot{\boldsymbol{\theta}} \end{pmatrix} + \begin{pmatrix} \mathbf{c}(\mathbf{q},\dot{\mathbf{q}}) + \mathbf{c}_1(\mathbf{q},\dot{\mathbf{q}},\dot{\boldsymbol{\theta}}) \\ \mathbf{c}_2(\mathbf{q},\dot{\mathbf{q}}) \end{pmatrix} + \begin{pmatrix} \mathbf{g}(\mathbf{q}) + \mathbf{K}(\mathbf{q}-\boldsymbol{\theta}) \\ \mathbf{K}(\boldsymbol{\theta}-\mathbf{q}) \end{pmatrix} = \begin{pmatrix} \mathbf{0} \\ \boldsymbol{\tau} \end{pmatrix} - \begin{pmatrix} \mathbf{D}(\dot{\mathbf{q}}-\dot{\boldsymbol{\theta}}) \\ \mathbf{D}(\dot{\boldsymbol{\theta}}-\dot{\mathbf{q}}) \end{pmatrix}, \quad (1)$$

where $\mathbf{M}$, $\mathbf{B}$, $\mathbf{c}_i$, $\mathbf{g}$, $\mathbf{K}$, and $\mathbf{D}$ are the link and actuator inertia matrix, Coriolis and centrifugal terms, gravity terms, joint stiffness, and damping matrices respectively. In (1), $\mathbf{q}$ and $\boldsymbol{\theta}$ are the link and motor side joint angles respectively, and $\boldsymbol{\tau}$ is the motor side torque. The link and motor side equations in (1) are coupled through the elastic torque $\boldsymbol{\tau}_J = \mathbf{K}(\boldsymbol{\theta} - \mathbf{q})$ at the joints and also via $\mathbf{S}(\mathbf{q})$ the low inertia coupling matrix. In (1), two factors have often been overlooked in the conventional elastic models that can potentially affect the accuracy of those models and these are discussed below:

1) *Low Inertia Coupling*: $\mathbf{S}$ is usually a constant in the planar case or zero in the case of robots which has 2 links with orthogonal joint axes. In other general cases, $\mathbf{S}$ is usually ignored due to large reduction ratios (100-150), which reduces the coupling effect of $\mathbf{S}$ [14]. This simplifies the elastic model significantly but it also reduces the model's accuracy to some extent. The exact effect of ignoring $\mathbf{S}$ on the elastic model's accuracy has never been studied extensively in complex robotic systems, and this has been done in this work.
2) *Simplified Harmonic Drive Model*: Another important term that is being traded off for simplicity is the $\mathbf{B}$ matrix which includes the models of various transmission elements used for each robot joint. Since harmonic drives are more common in the robotics field, they are considered here. HD includes three main components: a wave generator, flex spline, and cylindrical spline. Of the three components, flex spline is flexible, and the joint elasticity is mainly due to this component. Most of the elastic joint models [11]–[13] consider the elasticity parameters but ignore the inertia of input and output components of an HD. In few other models [10], input inertia is added to the rotor inertia, and the output element is assumed to be an integral part of the link which is connected to the HD output. The insufficiencies of these simplifications have been reported elaborately in [15]–[17] with more detailed HD models. The complexity of the HD model that needs to be considered in the elastic robot model to compute a relatively more accurate B matrix which in turn can result in a better representation of system dynamics is also studied in this work.

For this study, we have considered three different numerical models: 1) mod_1 with a simple HD model, 2) mod_2 with a relatively complex HD model, and 3) mod_3 with a complex HD model and $\mathbf{S}$. A virtual model (mod_{ad}) developed using MSC Adams software is used for comparison.

III. System Settings for Analysis

A manipulator with three non-coplanar elastic joints has been considered in this work to analyse the effect of low inertia coupling and HD model. The system has 3 movable links with a reach of 1.5 m and weighs 139 kg. A 3-dimensional (3D) model of the system is shown in Fig. 1a. The following are the unique features and some assumptions about the system which has been considered for this study:

- The actuators of joints 1 and 2 are mounted on link 1 to reduce the inertia of the moving links by keeping them close to the robot's base.
- The motion transmission from the joint actuators to their respective links is done in two stages: belt-pulley (stage-1) and HD system (stage-2).
- Due to the above arrangement of actuators, the harmonic drive output for joint 1 is taken from the cylindrical spline. Whereas for joints 2 and 3, the output is taken from the flex splines of their respective drives.
- The joints are considered to be frictionless in order to study the other effects.
- Both joint and drive flexibility, i.e., rotational elasticity along the XYZ axes is considered for all three joints.

The aforementioned features 1-3 are common in most commercial industrial manipulators such as ABB's IRB 1600, IRB 2400, IRB 140, etc. The reason for choosing a system with 3 joints is to maximize the effect of the two factors mentioned in Section II and at the same time maintain the system's complexity to a moderate level. While a single joint system reduces the effects of ignoring S and adopting a simple HD model, choosing a system with > 3DoF only increases the system's complexity. The contribution of adverse effects from joints beyond 3 is minimal due to the usage of lighter actuators and transmission systems.

A. Adams Model of the System

A virtual model of the manipulator is created using MSC Adams software along with the elasticity considered for each joint as shown in Fig. 1a. The virtual model includes the HD model but not the belt-pulley for each joint, and in the HD, the flex spline is modeled as a rigid body. These are done to keep the virtual model relatively simple and easy to use. The implementation of joint elasticity for a single joint in Adams is shown in Fig. 1b. In particular, the figure shows joint 3 connecting Link 2 and Link 3. In Fig. 1b, cylindrical spline is fixed to Link 2 and revolute joints are defined for rotor (R_{rotor}), wave generator (R_{WGen}), and flex spline (R_{FSpl}) keeping Link 2 as the reference. The motion transmission obtained due to the belt-pulley system is replicated by defining a coupler joint of ratio r_b between R_{rotor} and R_{WGen}. Similarly, the reduced motion due to HD is modeled by defining another coupler between R_{WGen} and R_{FSpl} with r_{hd} set as its transmission ratio. In the above coupler joints, R_{rotor} and R_{WGen} are taken as the driver joints. Since the drive compliance due to belt and HD is along the same axis (Z), they are combined and only its resultant is considered here. The joint and drive compliance along XYZ axes is modeled by defining a 6D bushing between Link 3 and Flex Spline 3. A bushing is a connection tool in Adams that can render 6D compliance (3 translational + 3 rotational) between any two rigid bodies. High stiffness and damping parameters are set for translational displacements, and for rotational compliances, the values are chosen based on the datasheets of HD and bearing systems.

IV. Manipulator Model with Joint and Drive Elasticity and Various HD Models

A. Manipulator Model with Joint and Drive Elasticity

The numerical model of the manipulator is developed considering the joint and drive flexibilities, the low inertia coupling between the actuators and links, and the HD model. Figure 2 shows the manipulator model with the reference frame for each joint (O_i), joint coordinates for the input motion by each rotor (θ_{mi}), output motion after a two-stage reduction (θ_i), and the link motion due to drive compliance (q_i) and joint compliance along $X(q_{ix})$ and $Y(q_{iy})$ axes. For the kinematic transformation between different joint reference frames, the Denavit-Hartenberg's (DH) parameters derived for the 3-joint manipulator shown in Table I are used. For instance, the representation of O_0 in terms of the ground or inertial reference frame O_G denoted by T_0^G can be computed as follows,

$$T_0^G = R_{\theta_0,z} \cdot Tr_{d_0,z} \cdot Tr_{a_0,x} \cdot R_{\alpha_0,x}, \tag{2}$$

where $R_{\theta_0,z}$ and $R_{\alpha_0,x}$ are 4 × 4 homogeneous matrices with a zero displacement vector and their rotational components

TABLE I
DENAVIT-HARTENBERG PARAMETERS OF A 3-JOINT MANIPULATOR

DH Frame	a_i	d_i	α_i	θ_i
O_0	0	0.285	0°	0°
O_1	0	0.15	-90°	θ_1
O_2	-0.75	-0.16	0°	θ_2 + 90°
O_3	-0.75	-0.0375	0°	θ_3 + 90°

being a 3D rotational matrix along z and x axis respectively. Similarly, $Tr_{d_0,z}$ and $Tr_{a_0,x}$ are homogeneous matrices with unit rotation matrix and the displacement vectors are $\begin{bmatrix} 0 & 0 & d_0 \end{bmatrix}^T$ and $\begin{bmatrix} 0 & 0 & a_0 \end{bmatrix}^T$ respectively.

To represent O_1 in terms of O_G, the joint compliance of joint 1 along X and Y axes should also be taken into account. As a result, T_1^G is computed as shown below:

$$T_1^G = T_0^G \cdot (R_{q_{1y},y} \cdot R_{q_{1x},x}) \cdot (R_{\theta_1,z} \cdot Tr_{d_1,z} \cdot Tr_{a_1,x} \cdot R_{\alpha_1,x}), \tag{3}$$

where the first expression (right side) is the homogeneous transformation of O_1 in terms of O_0 denoted by A_1. This is further transformed by the second expression representing joint 1 compliance along X and Y axes and finally transformed to the G frame by pre-multiplying with T_0^G.

The dynamic equation of the system considering both joint and drive flexibilities are computed using the well known Euler-Lagrange equation as shown below:

$$\frac{d}{dt}\frac{\partial L}{\partial \dot{\Theta}} - \frac{\partial L}{\partial \Theta} = \mathbf{f}, \tag{4}$$

where, L is the difference between the total kinetic and potential energy of the system, $\mathbf{f}$ is the generalized force vector, and $\Theta = \begin{bmatrix} \mathbf{q}_{ix} & \mathbf{q}_{iy} & \mathbf{q}_i & \boldsymbol{\theta}_i \end{bmatrix}^T$ is the generalized joint coordinate vector that includes the joint compliance, drive compliance, and reduced motion coordinates of all the joints. The total kinetic and potential energy of the system are computed as $K = \sum_{i=1}^{n_l}(K_i^l + K_i^r + K_i^{wg} + K_i^{fs} + K_i^e)$ and $P = \sum_{i=1}^{n_l}(P_i^l + P_i^r + P_i^{wg} + P_i^{fs})$ respectively. In the above equation, $K_i^{l,r,wg,fs}$ and $P_i^{l,r,wg,fs}$ represent the kinetic and potential energy of i^{th} link, rotor, wave generator, and flex spline respectively, n_l is the number of links, and K_i^e denotes the i^{th} joint stiffness. The computation of the above elements are explained briefly in [18].

Using (4), the total inertia matrix of the system $\mathbb{M} \in \mathbb{R}^{n \times n}$ can be computed as shown below:

$$\mathbb{M} = \frac{\partial d}{\partial \ddot{\Theta}}\left(\frac{d}{dt}\frac{\partial L}{\partial \dot{\Theta}}\right), \tag{5}$$

where $n = n_{jf} + n_{df} + n_a$ is the total DoF of the system considered in the model, in which, n_{jf} and n_{df} represents the joint and drive flexibilities, and the number of actuated joints is denoted by n_a. From $\mathbb{M}$ various equation of motion elements shown in (1) such as $\mathbf{M} \in \mathbb{R}^{n_{df} \times n_{df}}$, $\mathbf{S} \in \mathbb{R}^{n_{df} \times n_a}$, $\mathbf{B} \in \mathbb{R}^{n_a \times n_a}$, and $\mathbf{c}_i \in \mathbb{R}^{(n_{df}+n_a) \times 1}$ can be extracted as explained in [14]. With the above equation of motion elements extracted from $\mathbb{M}$, the complete dynamic equation of motion given in (1) is obtained in symbolic form for a 3-joint elastic manipulator. To evaluate the accuracy of the numerically computed model mod_3, that includes $\mathbf{S}$ and all HD components as defined in (1), a pre-defined joint

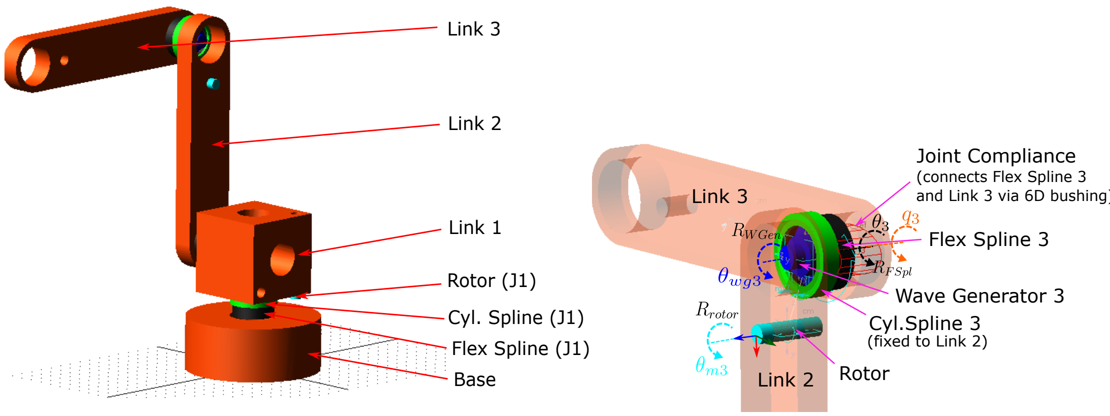

(a) (b)

Fig. 1. (a) A virtual model of a 3 joint elastic robot modelled in Adams. (b) Implementation of joint elasticity in Adams is shown here for joint 3 along with the rotor and harmonic drive components. θ_{m3}, θ_{wg3}, θ_3, and q_3 represents the position of rotor, wave generator, flex spline, and link respectively.

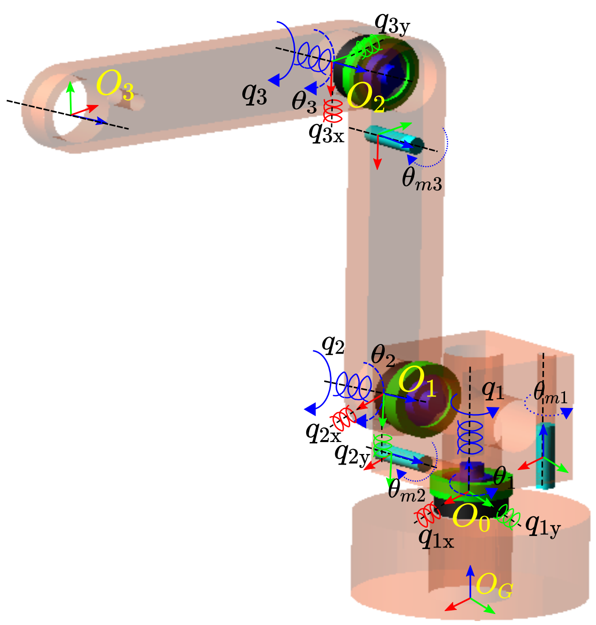

Fig. 2. A 3-joint elastic model of a manipulator is shown here with the joint reference frames, rotor motion, reduced motion after two stage reduction, link motion due to drive and joint compliance represented by O_i, θ_{mi}, θ_i, q_i, q_{ix}, and q_{iy} respectively. O_G denotes the ground or inertial reference frame of the model and the helical coils around XYZ axes show the rotational compliance along each axis.

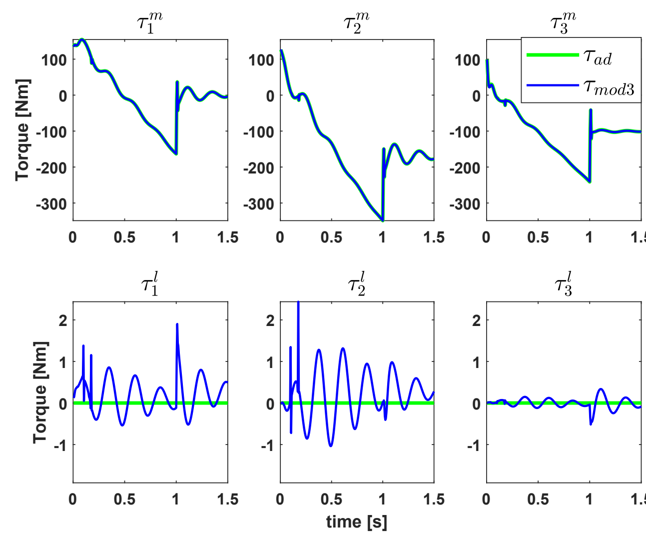

Fig. 3. Joint (τ_1^m, τ_2^m, τ_3^m) and link side torque (τ_1^l, τ_2^l, τ_3^l) values comparison made between the virtual model (mod_{ad}) and numerically computed model (mod_3) using (1), for a pre-defined joint motion.

motion is used to compute the joint (τ_1^m, τ_2^m, τ_3^m) and link-side torque (τ_1^l, τ_2^l, τ_3^l) values. These values are compared to those obtained with the virtual model (mod_{ad}) developed using Adams (see Fig. 2), as shown in Fig. 3. For the pre-defined motion, a step ramp of 0.1 rad on the output side of HD in $1s$ is used. The joint side torque values here refer to those obtained at the HD output. The r_b and r_{hd} considered for this motion are 3 and 121 respectively, resulting in a total transmission ratio (r_{tot}) of 363. This is the maximum value considered in this work to show the extreme possible errors in the numerical model. From Fig. 3, we can see that the τ_i^m of mod_3 correlate well to that of mod_{ad}. However, in the case of τ_i^l, the torque values computed using mod_3 are not exactly zero when compared to those obtained using mod_{ad}. This discrepancy is due to the 6 DoF bush joint modeled between flex spline and the link to represent the system's joint compliance in mod_{ad}, as shown in Fig. 1b.

B. Various Harmonic Drive Models

The conventional approach to model a HD system numerically is to consider the rotor and wave generator as a single component and the flex spline as part of the link that is being moved. Using this approach can result in erroneous torque results for the following reasons:

- The input motion from the rotor to the link is done in two stages: belt-pulley (stage-1) and HD (stage-2). This is unlike the conventional ones, where the rotor is directly connected to the HD's input component.
- Depending upon the transmission ratio of stage-1 reduction, the dynamics of the wave generator inferred at the rotor can vary considerably.
- The dynamic properties of HD components are considerably high for bigger systems, like the one considered here,

making it harder to ignore them.

- Finally, for applications that require high accuracy relatively more accurate HD models are required to capture its dynamics reliably.

On the other hand, there are also several complex HD models that have been reported in [16], [17], and they can capture more accurately the dynamics of systems which are harmonic driven. Though these models closely represent the harmonic drives, they are predominantly applied on 1 DoF systems Further, incorporating such complex HD models in multi-DoF joint elastic systems like the one considered in this work can make it too complex for computational reasons. As a result, two different models have been considered here, to determine the one which is less complex and at the same time accurate enough to capture joint dynamics.

1) HD Model With Only Wave Generator (mod_1): The first model considers the rotor and wave generator as individual components, and the cylindrical/flex spline is taken to be an integral part of the link that is attached to HD's output. In this case, the joint compliance is assumed to be before the flex spline, and the reflected inertia at the HD output (I_{hd}^{rfl}) and its resultant torque (τ_{hd}) are computed as

$$\begin{aligned} I_{hd}^{rfl} &= I_{wg} \cdot n_{hd}^2 + I_r \cdot r_b^2 \cdot r_{hd}^2, \\ \tau_{hd} &= \alpha_{wg} \times I_{hd}^{rfl}, \end{aligned} \tag{6}$$

where I_{wg} and I_r are the inertia of the rotor and wave generator respectively, and α_{wg} is the acceleration of the wave generator. The above reflected inertia form appears in the diagonal actuator inertia matrix, $\mathbf{B}$, for each joint i computed with their respective I_r^i and I_{wg}^i values. Since the cylindrical/flex spline components are not considered separately, the other equation of motion elements such as $\mathbf{M}$, $\mathbf{g}$, $\mathbf{c}$, and $\mathbf{c}_i$ also changes in (1). Due to the non-consideration of $\mathbf{S}$, it is taken to be a null matrix in (1) for mod_1.

2) HD Model With Wave Generator and Splines (mod_2): The second model is relatively more detailed when compared to the previous one, involving the splines of HD along with the rotor and wave generator components. The cylindrical/flex spline is considered to be a separate part, and it is coupled to the link through joint compliance. In this case, the reflected inertia at the HD output and its resultant torque are computed as given below

$$\begin{aligned} I_{hd}^{rfl} &= I_{spl} + I_{wg} \cdot r_{hd}^2 + I_r \cdot r_b^2 \cdot r_{hd}^2, \\ \tau_{hd} &= \alpha_{spl} \times I_{hd}^{rfl}, \end{aligned} \tag{7}$$

where I_{spl} and α_{spl} are the inertia and acceleration of cylindrical/flex spline depending upon the mounting arrangement of the HD. Since the cylindrical/flex spline component of HD is also considered in the model, all the equation of motion elements in (1) remain the same, except for $\mathbf{S}$, which is taken to be a null matrix since it is ignored here.

C. Effect of Adopting a Simplified HD Model

The τ_i^m and τ_i^l values computed for the pre-defined joint motion (Fig. 3) using three different numerical models: mod_1, mod_2, and mod_3 are compared in Fig. 4a. From the figure, we can observe a close correspondence of τ_i^m values between mod_1, mod_2, and mod_3. In the case of τ_i^l, mod_1 and mod_2 differ slightly from mod_3 with the former showing large variation. This is attributed to the fact that the S term is not considered in mod_1 and mod_2. Between mod_1 and mod_2 also some difference is observed due to the different way of modeling the HD system. To quantify the differences between the models and make an efficient comparison, two performance metrics on the torque values have been considered here: maximum error (e_{max}) and root mean square error (e_{rmse}). Both e_{max} and e_{rmse} are computed with respect to mod_3.

To understand how the HD model error propagates as the transmission ratio is increased, five different r_{tot} values (5, 51, 128, 230, and 363) have been considered for the performance metric comparisons shown in Fig. 4b. As observed in Fig. 4a, the difference between mod_1 and mod_2 is very minimal for the τ_i^m values as r_{tot} is increased. The reason can be visualized by comparing the computation of I_{hd}^{rfl} in mod_1 and mod_2, as seen in (6) and (7) respectively. The main difference is the inclusion of I_{spl} in (7) but its effect is relatively minimal since the rest of the terms are multiplied by r_b^2 and r_{hd}^2. The difference is relatively more pronounced in τ_1^m because HD output is at the end of the cylindrical spline instead of the flex spline, and the former's inertia is 10 times higher than the latter. This is due to a different arrangement of the HD assembly for joint 1.

On the other hand, the difference between mod_1 and mod_2 is more pronounced on τ_i^l values and the latter reporting relatively less error. This is due to the less accurate modeling of HD in mod_1 since it doesn't include the spline components of HD. The modeling error appears predominantly through the $\mathbf{M}(\mathbf{q})$ and $\mathbf{c_i}$ terms because of the absence of I_{spl} in those terms in mod_1, which is not the case with mod_2. The error in mod_1 and mod_2 and their inter differences increases linearly as r_{tot} increases for joint 1 and 2. The causality of this can be visualized in (1), in which one of the $\mathbf{c_i}$ is a function of $\dot{\theta}$ and it is related to the rotor angular velocity $\dot{\theta}_m$ as $\dot{\theta} = r_{tot} \cdot \dot{\theta}_m$. The error observed in mod_2 for joint 1 and 2 is mainly due to the absence of the $\mathbf{S}$ term. In the case of joint 3, the performance metric error remains constant for mod_1 as r_{tot} is increased, and is 0 for mod_2. The former trend suggest that the error is mainly through $\mathbf{M}(\mathbf{q})$ due to the ignorance of I_{spl} because of simple HD model in mod_1. Since joint 3 is the last one and there are no relatively moving bodies, the components corresponding to τ_3^l in $\mathbf{c_i}$ and $\mathbf{S}$ are 0.

V. Effect of Ignoring Low Inertia Coupling

The effect of excluding spline components in the HD model and ignoring the $\mathbf{S}$ matrix can be analyzed by comparing mod_3 with the other two models mod_1 and mod_2. mod_3 includes the detailed HD model of mod_2, and it also considers $\mathbf{S}$. For the system considered here, the computed $\mathbf{S}$ matrix looks like the following:

$$S = \begin{pmatrix} S_{1,1} & S_{1,2} & S_{1,3} \\ 0 & 0 & S_{2,3} \\ 0 & 0 & 0 \end{pmatrix}, \tag{8}$$

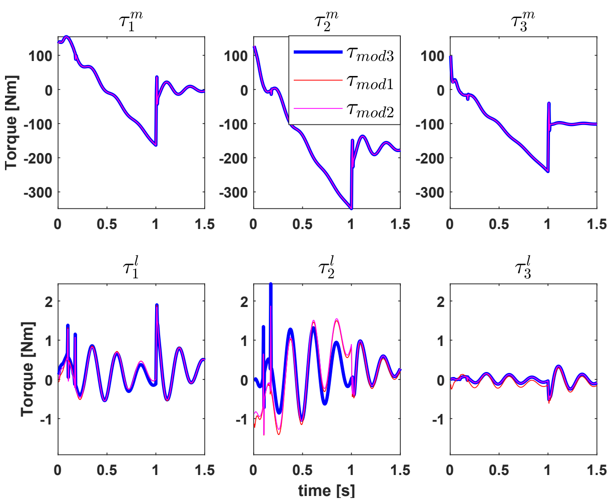

(a)

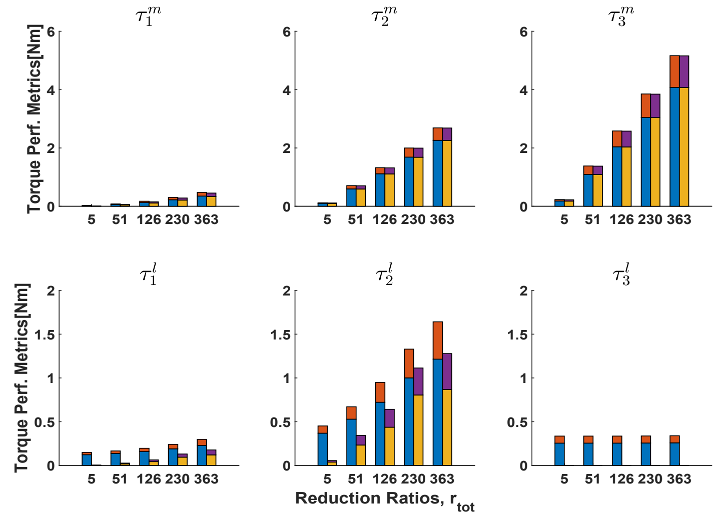

(b)

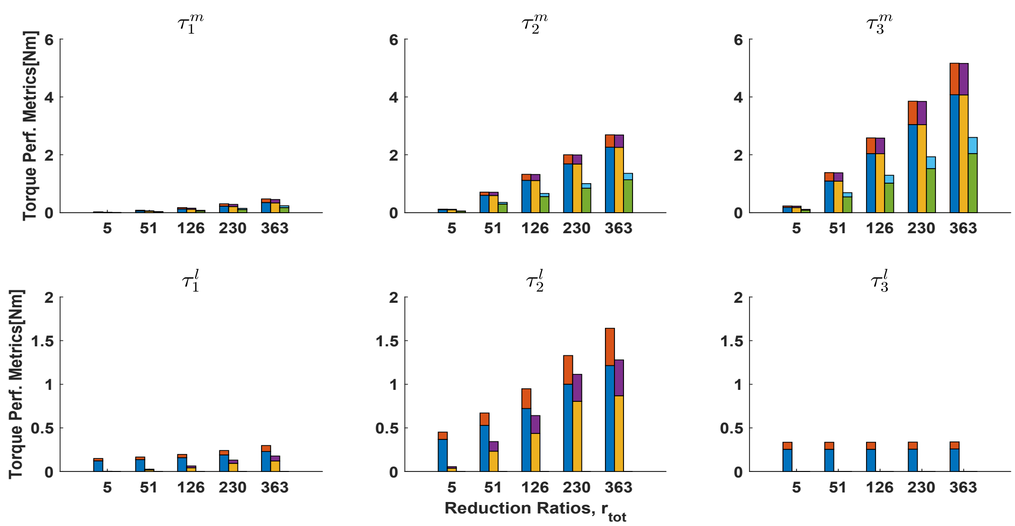

(c)

Fig. 4. (a) Joint and link side torque obtained for a pre-defined motion using three different models are shown here. The three different models considered here are: simple HD model (mod_1), relatively complex HD model (mod_2), and complex HD model with low inertia coupling (mod_3). (b) The performance metrics (maximum error(e_{max}) and root mean square error (e_{rmse})) of the joint and link side torque values computed with different reduction ratios are compared here between mod_1 (1st stacked bar) and mod_2 (2nd stacked bar). In each stacked bar, the bottom and top bars represent e_{max} and e_{rmse} respectively. (c) Comparison of torque performance metrics made between mod_1, mod_2, and mod_3 (3rd stacked bar).

with
$$\begin{aligned} S_{1,1} &= I_{zz}^{r,1} r_b r_{hd} \sigma_1, \\ S_{1,2} &= I_{zz}^{fs,2}\sigma_2 + I_{zz}^{wg,2} r_{hd}\sigma_2 + I_{zz}^{r,2} r_b r_{hd}\sigma_2, \\ S_{1,3} &= I_{zz}^{fs,3}\sigma_3 + I_{zz}^{wg,3} r_{hd}\sigma_3 + I_{zz}^{r,3} r_b r_{hd}\sigma_3, \\ S_{2,3} &= I_{zz}^{fs,3}\sigma_4 + I_{zz}^{wg,3} r_{hd}\sigma_4 + I_{zz}^{r,3} r_b r_{hd}\sigma_4. \end{aligned} \tag{9}$$

In (9), coefficients which are functions of $\mathbf{q}$ are represented in the form of σ_i for brevity.

Similar to Fig. 4b, the performance metrics of τ_i^m and τ_i^l values are compared in Fig. 4c between the three models to understand the aforementioned effect. The performance metric of τ_i^m values computed with mod_3 are much better than those computed using mod_1 and mod_2. Both e_{max} and e_{rmse} of mod_3 increases linearly as the r_{tot} is increased but they are ≈50% less when compared to those of other models. The significant improvement in the accuracy is due to the inclusion of $\mathbf{S}$ in mod_3 as shown in (1), and this is not the case with mod_2 and mod_1. However, torque due to the rotor and HD component's inertia, which are part of the $\mathbf{B}$ term, dominate significantly since they are multiplied by r_b and r_{hd} as shown in (7).

In the case of τ_i^l, both e_{max} and e_{rmse} are very minimal because of the consideration of $\mathbf{S}$ term in mod_3 as seen in (1). This is replaced by a null matrix $\mathbf{0}$ in the case of mod_1 and mod_2 to achieve a simplified model. Hence, the values computed with mod_3 are relatively more accurate than the others. Since the elements in $\mathbf{S}$ corresponding to τ_3^l are 0 as observed in (8) both mod_2 and mod_3 values of τ_3^l match exactly. The constant error observed with mod_1 for τ_3^l is due to the exclusion of spline component in its HD model.

VI. Estimation Error of Different Models

Sections IV-B and V demonstrate the likely error to occur in the joint and link-side torque values due to different models, but the relative torque error appears to be minimal. To understand its exact impact, it is necessary to assess the effect of each model's torque errors in estimating their respective dynamic parameters Ψ, i.e., the mass, center of mass, inertia of different components, and the stiffness and damping of joints. Few works have already been proposed to estimate the dynamic parameters of a manipulator, such as [6], [7], [19], etc. In this work, we have adapted the estimation procedure proposed in [6] for our elastic joint model. For the estimation here, we have set $\mathbf{q}_{ix}$, $\mathbf{q}_{iy}$, and their respective derivatives to 0. The elements of equation of motion shown in (1) $\mathbf{M}(\mathbf{q})$, $\mathbf{S}(\mathbf{q})$, $\mathbf{B}$, $\mathbf{g}(\mathbf{q})$, $\mathbf{K}(\mathbf{q},\boldsymbol{\theta})$, $\mathbf{D}(\dot{\mathbf{q}},\dot{\boldsymbol{\theta}})$, and $\mathbf{c}_i(\mathbf{q},\dot{\mathbf{q}},\dot{\boldsymbol{\theta}})$ are all functions of the dynamic parameters Ψ. Since the aforementioned elements are also functions of $\mathbf{q}$, $\dot{\mathbf{q}}$, $\ddot{\mathbf{q}}$, $\boldsymbol{\theta}$, $\dot{\boldsymbol{\theta}}$, and $\ddot{\boldsymbol{\theta}}$, they can be rewritten in a linear regression form as shown below

$$[\mathbf{0} \quad \boldsymbol{\tau}]^T = \Phi(\mathbf{q},\dot{\mathbf{q}},\ddot{\mathbf{q}},\boldsymbol{\theta},\dot{\boldsymbol{\theta}},\ddot{\boldsymbol{\theta}})\Psi, \quad (10)$$

where Φ is the regression or identification matrix, and Ψ is the dynamic parameter vector that needs to be estimated, and this is observed to be linear as seen in (10). Φ can be computed easily since it is a function of motion parameters.

A. Dynamic Parameters and Coefficients Estimation

To estimate the parameters reliably, it is necessary to design motions that can sufficiently excite the parameters which are to be estimated. We have used a parametric way based on the Fourier series to design trajectories, and the parameters are optimized using a pattern search algorithm from Matlab. For more details please refer to [5]. The resulting optimal excitation trajectory is used to simulate the virtual Adams model, and the corresponding joint and link-side torque values are recorded. Using the linear regression form in (10), the parameter/coefficient vector Ψ can be estimated in a linear least-square form Ψ_{ls} as follows:

$$\Psi_{ls} = (\mathbf{F}^T\mathbf{F})^{-1}\mathbf{F}^T\mathbf{b}, \quad (11)$$

with

$$\mathbf{F} = \begin{bmatrix} \Phi(\mathbf{q},\dot{\mathbf{q}},\ddot{\mathbf{q}},\boldsymbol{\theta},\dot{\boldsymbol{\theta}},\ddot{\boldsymbol{\theta}})^1 \\ \cdots \\ \cdots \\ \Phi(\mathbf{q},\dot{\mathbf{q}},\ddot{\mathbf{q}},\boldsymbol{\theta},\dot{\boldsymbol{\theta}},\ddot{\boldsymbol{\theta}})^{N_s} \end{bmatrix}, \quad \mathbf{b} = \begin{bmatrix} [0 \quad \boldsymbol{\tau}]_1^T \\ \cdots \\ \cdots \\ [0 \quad \boldsymbol{\tau}]_{N_s}^T \end{bmatrix} \quad (12)$$

is the measured torque vector collected for N_s samples. For the estimation here, 100 samples are collected at a frequency of 10Hz over a trajectory duration of 10 secs. Due to the linear dependency of some of the columns in the $\mathbf{F}$ matrix, few parameters can only be estimated in a linear combination with other parameters, i.e., dynamic coefficients [20].

Following the parameter estimation procedure, the different models are rewritten in their respective standard regression forms, as shown in (10). This is followed by the least square estimation of each model's dynamic parameters using (11). Since the $\mathbf{F}$ matrix is likely to differ for different models, the estimated Ψ_{ls} can also vary for various models. The total number of parameters that can be estimated with mod_2 and mod_3 are 75, and for mod_1 it drops down to 65. The parameters that cannot be estimated with mod_1 are the mass and inertia of cylindrical/flex spline components. This is due to the assumption of a relatively simple HD model, as discussed in Section IV-B. In the case of mod_1 and mod_2, though the actual number of parameters that can be estimated is the same, most of them are estimated in a linearly combined form, and hence, they are likely to differ.

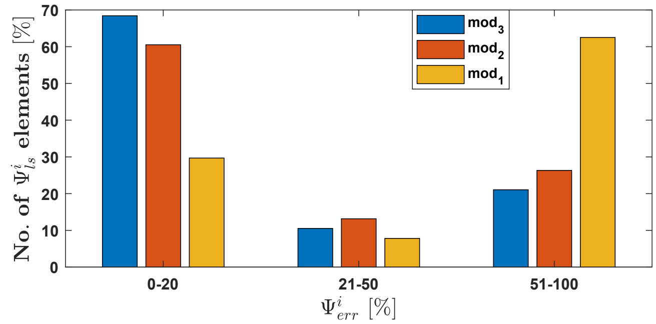

Fig. 5. The Ψ^i_{err} is categorized into three categories (0-20%, 21-50%, and 51-100%) and the percentage of Ψ^i_{ls} elements falling under each category is compared across three models: mod_1, mod_2, and mod_3.

B. Comparison of Relative Estimation Error (Ψ_{err})

In order to deduce the estimation error for each model i, the true Ψ^i vector is computed for each one using the actual values of the dynamic parameters, and the relative estimation error vector Ψ^i_{err} in percentage is computed as shown below:

$$\Psi^i_{err} = ((\Psi^i_{ls} - \Psi^i)/\Psi^i) \times 100. \quad (13)$$

Again, the individual elements of Ψ^i_{err} of different models cannot be compared directly due to the number of parameters and its various linear combinations. Hence, the overall estimation accuracy of mod_1, mod_2, and mod_3 are compared by segregating the error into three categories: low (0-20%), mid(21-50%), and high (51-100%). Figure 5 compares the percentage of Ψ^i_{ls} elements computed for each model mod_i falling under three different error categories. From the figure, we can see that the relatively simple model mod_1 estimates 62.5% of Ψ^i_{ls} with high error, and only 29.69% of them are estimated with low error. This trend is associated with the fact that mod_1 uses a relatively simple HD model and also ignores the $\mathbf{S}$ term. In the case of mod_2 and mod_3, though both the models can estimate the same number of parameters, mod_2 doesn't consider the $\mathbf{S}$ term. As a result, mod_3 reports a higher percentage (68.42%) of Ψ^i_{ls} estimated with low error when compared to mod_2 which reports a slightly lower value (60.53%). However, with mod_2 and mod_3, a significantly higher percentage of Ψ^i_{ls} can be estimated with a lower error when compared to mod_1. Also, a significantly lower percentage of Ψ^i_{ls} have been estimated with high error using mod_2 (26.32%) and mod_3 (21%) when compared to that of mod_1. In the mid-range error category, the difference between different models seems to be minimal, with mod_2 reporting a slightly higher value of 13.16%. Overall, mod_2 and mod_3 estimate more number of Ψ^i_{ls} with lower error, and of which mod_3 being the relatively accurate model performs better across different error categories.

VII. Discussion and Conclusion

1) Discussion: For this study, we haven't considered any sensor noises, and this may have some minor effects on the reported results. The noise effect will be minor because for the estimation reported in Section VI we require only joint encoders and joint torque sensors. Joint velocity and accelerations can be analytically estimated instead of offline differentiation, thanks to the use of the Fourier series wave to design the excitation trajectories. Of the two sensors, joint torque sensors are notorious for noisy measurements. Assuming a white Gaussian noise (μ = 0, σ = 0.26 Nm) for torque sensors [21], only the results reported for τ^m_1 in Fig. 4b and Fig. 4c are most likely to be dominated by noise since the maximum value is < 0.5 Nm across different r_{tot}.

In Section VI, most of the elements of Ψ_{ls} are estimated in a linear combination of dynamic parameters, except for a few. Though it is possible to estimate the individual parameters from their linear combinations using non-linear optimization [20], we have chosen Ψ_{err} for comparison in Section VI-B Even if the individual parameters are extracted from Ψ_{ls} using [20], the overall results and observations drawn in Section VI-B may not change significantly since the extraction error is still limited by the accuracy of Ψ_{ls}. However, it will certainly give us more information about the exact estimation error of each parameter. Further, in Fig. 5, even for mod_2 and mod_3 around 20-30% of Ψ_{ls} have estimation error percentage $>$ 51%. This is because the elements of Ψ_{ls} are in a linear combination of inertia, CoM, and mass of various components, and they are likely to result in low values due to the lower values of inertia and CoM. As a result, even a small change in ψ^i_{ls} can result in high ψ^i_{err} for each model as computed in (13).

2) Conclusion: In this work, the effect of ignoring **S** and adopting a simple HD model on the accuracy of a joint elastic model of an industrial manipulator has been studied. Three different models are considered here for comparison: mod_1, mod_2, and mod_3. The torque performance metric computed across different reduction ratios for all three models reported a relatively better accuracy of mod_3. Though the torque difference between the models seems to be minimal, using these models to estimate the system's dynamic parameters/coefficients resulted in a considerable error, with mod_3 having a relatively better estimation. The proposed detailed elastic model mod_3 can improve the manipulator's accuracy reported in [11], [12], [22] Experimental verification of this will be carried out in our future work.

References

[1] H. Olsen and G. Bekey, "Identification of robot dynamics," in *Proceedings. 1986 IEEE International Conference on Robotics and Automation*, vol. 3. IEEE, 1986, pp. 1004–1010.

[2] P. K. Khosla and T. Kanade, "Parameter identification of robot dynamics," in *1985 24th IEEE Conference on Decision and Control*. IEEE, 1985, pp. 1754–1760.

[3] M. Gautier and W. Khalil, "On the identification of the inertial parameters of robots," in *Proceedings of the 27th IEEE Conference on Decision and Control*, vol. 3. IEEE Austin, 1988, pp. 2264–2269.

[4] ——, "Exciting trajectories for the identification of base inertial parameters of robots," *The International journal of robotics research*, vol. 11, no. 4, pp. 362–375, 1992.

[5] J. Swevers, C. Ganseman, D. B. Tukel, J. De Schutter, and H. Van Brussel, "Optimal robot excitation and identification," *IEEE transactions on robotics and automation*, vol. 13, no. 5, pp. 730–740, 1997.

[6] J. Swevers, W. Verdonck, and J. De Schutter, "Dynamic model identification for industrial robots," *IEEE control systems magazine*, vol. 27, no. 5, pp. 58–71, 2007.

[7] C. Gaz, M. Cognetti, A. Oliva, P. R. Giordano, and A. De Luca, "Dynamic identification of the franka emika panda robot with retrieval of feasible parameters using penalty-based optimization," *IEEE Robotics and Automation Letters*, vol. 4, no. 4, pp. 4147–4154, 2019.

[8] Z.-H. Jiang, T. Ishida, and M. Sunawada, "Neural network aided dynamic parameter identification of robot manipulators," in *2006 IEEE international conference on systems, man and cybernetics*, vol. 4. IEEE, 2006, pp. 3298–3303.

[9] E. Burdet and A. Codourey, "Evaluation of parametric and nonparametric nonlinear adaptive controllers," *Robotica*, vol. 16, no. 1, pp. 59–73, 1998.

[10] A. Albu-Schaffer and G. Hirzinger, "Parameter identification and passivity based joint control for a 7 dof torque controlled light weight robot," in *Proceedings 2001 ICRA. IEEE International Conference on Robotics and Automation (Cat. No. 01CH37164)*, vol. 3. IEEE, 2001, pp. 2852–2858.

[11] J. Öhr, S. Moberg, E. Wernholt, S. Hanssen, J. Pettersson, S. Persson, and S. Sander-Tavallaey, *Identification of flexibility parameters of 6-axis industrial manipulator models*. Linköping University Electronic Press, 2006.

[12] M. Neubauer, H. Gattringer, A. Müller, A. Steinhauser, and W. Höbarth, "A two-stage calibration method for industrial robots with joint and drive flexibilities," *Mechanical sciences*, vol. 6, no. 2, pp. 191–201, 2015.

[13] T. Hardeman, *Modelling and identification of industrial robots including drive and joint flexibilities*. Universiteit Twente, 2008.

[14] B. Siciliano and O. Khatib, "Chapter 13: Robots with flexible joints," in *Springer handbook of robotics*. Springer, 2016, pp. 287–319.

[15] T. D. Tuttle and W. Seering, "Modeling a harmonic drive gear transmission," in *[1993] Proceedings IEEE International Conference on Robotics and Automation*. IEEE, 1993, pp. 624–629.

[16] W. Seyfferth, A. Maghzal, and J. Angeles, "Nonlinear modeling and parameter identification of harmonic drive robotic transmissions," in *Proceedings of 1995 IEEE International Conference on Robotics and Automation*, vol. 3. IEEE, 1995, pp. 3027–3032.

[17] P. Folega, G. Wojnar, R. Burdzik, and Ł. Konieczny, "Dynamic model of a harmonic drive in a toothed gear transmission system," *Journal of Vibroengineering*, vol. 16, no. 6, pp. 3096–3104, 2014.

[18] M. W. Spong and M. Vidyasagar, "Chapter 9: Dynamics," in *Robot dynamics and control*. John Wiley & Sons, 2008.

[19] L. Zollo, E. Lopez, L. Spedaliere, N. Garcia Aracil, and E. Guglielmelli, "Identification of dynamic parameters for robots with elastic joints," *Advances in Mechanical Engineering*, vol. 7, no. 2, p. 843186, 2015.

[20] C. Gaz, F. Flacco, and A. De Luca, "Extracting feasible robot parameters from dynamic coefficients using nonlinear optimization methods," in *2016 IEEE international conference on robotics and automation (ICRA)*. IEEE, 2016, pp. 2075–2081.

[21] N. Kashiri, J. Malzahn, and N. G. Tsagarakis, "On the sensor design of torque controlled actuators: A comparison study of strain gauge and encoder-based principles," *IEEE Robotics and Automation Letters*, vol. 2, no. 2, pp. 1186–1194, 2017.

[22] C. Gong, J. Yuan, and J. Ni, "Nongeometric error identification and compensation for robotic system by inverse calibration," *International Journal of Machine Tools and Manufacture*, vol. 40, no. 14, pp. 2119–2137, 2000.